Influence of cross section loss on the stress-strain characteristics of corroded quenched and self-tempered reinforcing bars

Journal Article

Author(s):
Häfliger, Severin; Kaufmann, Walter

Publication date:
2021-05-03

Permanent link:
https://doi.org/https://doi.org/10.3929/ethz-b-000473486

Originally published in:
Construction and Building Materials 282, https://doi.org/10.1016/j.conbuildmat.2021.122598

Construction and Building Materials 282 (2021) 122598

Contents lists available at ScienceDirect

Construction and Building Materials

journal homepage: www.elsevier.com/locate/conbuildmat

Influence of cross section loss on the stress-strain characteristics of corroded quenched and self-tempered reinforcing bars

Severin Haefliger *, Walter Kaufmann

Institute of Structural Engineering, ETH Zurich, 8093 Zurich, Switzerland

HIGHLIGHTS

- Stress-strain behaviour of microstructure layers were determined experimentally.
- Constitutive relations for perlitie/ferrite, bainite and martensite were deduced.
- A simple model allows to calculate full stress-strain curve of composed QST rebar.
- Uniform corrosion leads to strong reduction of load-bearing capacity for QST rebars.
- Load-bearing capacity is not significantly reduced in case of pitting corrosion.

GRAPHICAL ABSTRACT

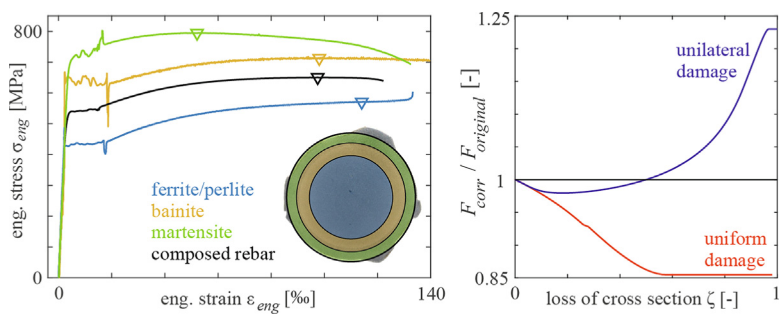

ARTICLE INFO

Article history:
Received 20 October 2020
Received in revised form 10 January 2021
Accepted 2 February 2021

Keywords:
Reinforcing bars
Tempcore
Thermomechanically treated
Quenched and self-tempered
Microstructure
Corrosion
Constitutive modelling

ABSTRACT

Many ageing reinforced concrete structures are affected by severe damage of reinforcing bars due to corrosion. Accurate knowledge of the stress-strain characteristics of the installed reinforcing bars is an indispensable prerequisite for the realistic assessment of the structural safety of such structures. The reduction in cross section does not only reduce the load bearing capacity of the reinforcing bars, but in case of hot-rolled, quenched and self-tempered (QST, process branded as "Tempcore®" or "Termex®") reinforcing bars also changes their structural characteristics. Since these bars exhibit three distinct microstructures in core, transition zone and outer annulus, each with different mechanical characteristics, the overall stress-strain behaviour of a corroded QST reinforcing bar depends on the composition of its residual area, which varies significantly with ongoing corrosion. As QST reinforcement is widely used in concrete structures worldwide, this effect is of high importance for any structural safety assessment of structures affected by corrosion.

This study investigates the influence of microstructure on strength and ductility of QST reinforcing bars subjected to axisymmetric cross section loss. In a comprehensive experimental campaign, 31 tensile tests on QST reinforcing bars with continuously reduced diameters were conducted, exploring the contribution of the concentric layers of the cylindrical cross section to the overall behaviour. Experimental results indicate a pronounced variation of strength and ductility over the cross section. Based on these observations, a simplified model was developed for the relationship between loss of cross section and mechanical characteristics. A validation shows excellent agreement between model and experimental data.

* Corresponding author.
E-mail address: haefliger@ibk.baug.ethz.ch (S. Haefliger).

https://doi.org/10.1016/j.conbuildmat.2021.122598
0950-0618/

1. Introduction

1.1. Overview of the effects of corrosion and on the focus of this study

The reinforcement of many ageing concrete structures is affected by local and /or uniform reinforcement corrosion due to chloride attack and carbonation, respectively. Corrosion reduces the residual load-bearing capacity by several mechanisms [1–3]. These affect the reinforcement, the concrete, and the interaction between reinforcement and concrete. The initial passive layer of the reinforcement, caused by the high alkalinity of concrete, is either attacked by carbonation of concrete or the presence of chlorides, leading to a uniform or local reduction of the reinforcing bars' cross section, respectively. Subsequently, concrete may be damaged by splitting or spalling due to the volume expansion of the corrosion products [2–4], leading to a reduction of concrete area. Furthermore, bond between reinforcement and concrete is reduced as a result of the reduced cross section of the reinforcing bars, lubricating effects of the corrosion products, and the presence of cracks parallel to the reinforcement [4–6], which potentially leads to e.g. anchorage failures and larger crack openings.

Given this multitude of corrosion effects, the structural safety of corroded structures clearly does not depend exclusively on the residual mechanical properties of the corroded reinforcing bars. Nonetheless, accurate knowledge of the stress–strain characteristics of damaged reinforcing bars is a prerequisite to determine the load-bearing and deformation capacity of corroded structures. The following main effects on this behaviour were identified by the authors: (i) the applied strain rate [7–9]; (ii) various steel microstructures within the cross section in quenched and self-tempered (QST) reinforcing bars [10–14]; (iii) a three-dimensional stress state near the damage zone for local corrosion [15]; and (iv) bending effects for localised corrosion pits due to a shift in the neutral axis [15,16].

The present paper addresses the effect of cross section loss on the stress–strain characteristics of QST reinforcing bars, which contain distinct microstructure layers within their cross section, focusing on the differences in the mechanical characteristics of the distinct layers. Due to these differences, QST reinforcing bars alter their overall mechanical behaviour continuously when corroding, depending on the ratio of areas of the residual layers. Few studies [11,12] focused on this effect, and only one recent study [10] succeeded in giving a sound mechanical explanation of the resulting stress-strain behaviour.

In order to isolate this influence from the remaining effects, which are closely related to the geometry of the corroded reinforcing bars and have to be superimposed later on, an experimental campaign on reinforcing bars with axisymmetrically reduced cross section was carried out. The experiments indicate a pronounced variation of strength and ductility over the cross section. Based on these findings, a simplified model is developed to describe the relationship between loss of cross section and mechanical characteristics.

1.2. Effects not considered in this study

The further effects (i, iii, iv) mentioned above are beyond the scope of the present paper. The effect of strain rate (i), known for decades, has been revisited and complemented by data for modern reinforcing steels in a parallel study, and is discussed in a companion paper [9]. Three-dimensional stress-states (iii) and bending effects (iv), which are closely related to the geometry of the corroded reinforcing bar and particularly relevant for natural corrosion, are briefly discussed in the following, along with two additional aspects specific to QST reinforcing bars.

Doubtlessly, reinforcing bars embedded in concrete do not corrode axisymmetrically along the bar axis, particularly in the case of pitting corrosion. Despite the widely recognised importance of the pit geometry for the residual reinforcement characteristics, in most studies, the implications of corrosion are treated by means of statistical approaches [17–21], correlating the global mass loss with the global mechanical properties of the reinforcing bars; this is clearly of limited use for local corrosion. Only few studies [16,22–25] consider the variation of the mechanically relevant geometrical properties of corroded reinforcing bars (A_{eff}, I_{yy}, I_{zz}), and even less [16,23,25] correlate these properties with experimental results from tensile tests. To the authors' knowledge, Hingorani et al. [15] were the only ones who theoretically studied the effects of bending due to non-axisymmetric corrosion, and investigated the presence of a three-dimensional stress state for localised corrosion. Such investigations on a sound mechanical basis are essential to understand the implications of the pit geometry on the mechanical characteristics of corroded reinforcing bars. Authors are currently working on appropriate models following this approach.

In QST reinforcing bars, corrosion implies further, potentially negative effects on the load-deformation behaviour apart from the different mechanical characteristics of the distinct layers studied in this paper. These effects include a different corrosion behaviour than observed for reinforcing bars with uniform microstructure [26], affecting the pit geometry and hence, the local mechanical behaviour. Furthermore, the production process may cause surface micro cracks and impurities within the microstructure, which in combination with chloride ingress have been associated with stress corrosion [13,14]. Some studies also point to possible issues related to a potential instability between the different phases of QST reinforcing bars [14,27]. All these effects are, however, beyond the scope of the present paper.

1.3. Production processes and related implications of cross section loss

Today, mainly two production processes for reinforcing bars are used: Hot-rolling and cold-working (CW) and hot-rolling, quenching and self-tempering (QST). In the CW process, the hot-rolled reinforcing bar slowly cools down after the last rolling, which leads to a homogeneous microstructure over the cross section, consisting of a mixture of ferrite and perlite with high ductility but low yield stress. To increase the strength, bars are mechanically stretched (cold-worked) after cooling. Due to the plastic deformation induced by the process, such reinforcing bars lack a pronounced yield plateau and exhibit a lower strain at peak stress, as well as a reduced strain hardening, i.e. a lower ratio of tensile strength to yield stress.

Though first produced already in the 1970s [28], QST reinforcing bars have drawn attention only recently, as they are produced in large quantities mainly since the early 1990s. In the QST process, the hot-rolled reinforcing bar undergoes a brief, controlled water cooling (quenching), which leads to the formation of high strength, low ductile martensite at the outer part of the bar. This outer annulus of the cross section is then tempered by the still hot ferritic/perlitic core with lower strength but high ductility. The final reinforcing bar is a composition of ferrite/perlite in the core, bainite in the transition zone and martensite in the outer annulus, combining the mechnical characteristics of these steel microstructures. Hence, a pronounced yield plateau, a higher strain at peak stress and a higher strain hardening are observed for this type of reinforcing bar. Due to these favourable characteristics and the efficient production process, QST reinforcing bars have become the most used type of reinforcement in many regions worldwide.

The mechanical characteristics of QST reinforcing bars with inhomogeneous microstructure over their cross section thus depend on the characteristics of the different steel microstructures and their relative areas. If a reinforcing bar is damaged, e.g. due to corrosion, its mechanical characteristics alter – continuously in case of progressing corrosion –, starting at the martensitic outer annulus with its higher strength. Hence, the reduction in load-bearing capacity is higher than the loss of cross section. Accurate knowledge of the behaviour of damaged QST reinforcing bars is thus essential to accurately assess the residual load-bearing and deformation capacity of structures affected by corrosion.

1.4. Current state of research on the static implications of the different microstructures for QST reinforcing bars

Fernandez et al. [11] carried out tensile tests on QST reinforcing bars with initial diameter Ø12 mm and various reduced diameters, and reported variable strengths of the layers (annuli) over cross section. They succeeded in calculating the yield stress and tensile strengths of each layer and built up a model based on these stress values. However, they completely ignored the influence of the differing microstructure composition on the ductility of the reinforcing bar. Santos and Henriques [12] conducted tensile and hardness tests on QST reinforcing bars with initial diameter Ø20 mm and various reduced diameters. They reported the yield stress and tensile strength of the specimens and the hardness over the diameter, which allows determining the boundaries of the distinct microstructure layers. Additionally, the observed strains at yielding and peak stress are documented, but results did not indicate any variation regarding the distinct layers. Cadoni et al. [29] thoroughly investigated the hardness over the diameter of a QST reinforcing bar Ø40 mm, including a specification of the microstructure. Moreover, they extracted samples of diameter Ø6 mm and 40 mm length out of the different layers, on which they performed tensile tests. They provide stress–strain diagrams of the different layers, clearly indicating the higher strength and lower ductility of the outer annulus compared to the core and the undamaged reinforcing bar. Rocha et al. [30] performed hardness tests over the diameter and a specification of the microstructure. Hortigón Fuentes et al. [10] performed Vickers hardness tests over the diameter and tensile tests on QST reinforcing bars with an initial diameter Ø14 mm and with reduced diameter. To the authors' knowledge, they were the first and so far only to comprehensively report and discuss the behaviour of the distinct microstructure layers, providing some stress–strain diagrams of the layers' behaviour as well as a finite element model.

Although the importance of the topic has been recognised by the research community about a decade ago and several studies and experimental campaigns were carried out, a sound mechanical modelling approach for the influence of the distinct microstructure on the behaviour of corroded QST reinforcing bars was established only recently [10]. This study presents a similar, but more general approach of a consistent mechanical model, which is based on the experimental results of the conducted tensile tests. It is capable of representing the stress-strain behaviour of the distinct microstructure layers and the thereof composed reinforcing bar. The model therefore allows investigating the effects of inhomogeneous microstructure for corroded QST reinforcing bars without any restraints regarding damage geometry. Nevertheless, it is important to notice that other relevant effects in case of pitting corrosion (pit geometry, impurities in microstructure) are not investigated in this study and thus not covered by the model.

2. Experimental programme

The experimental campaign was carried out in the structural laboratory at ETH Zurich and comprised 31 specimens of QST reinforcing bars, similar to those investigated in [9]. The specimens with a nominal (initial) diameter of 20 mm were all taken from the same production batch. Over a length of 250 mm, their cross section was reduced axisymmetrically by machining on a lathe (turning) to target remaining diameters of 10 mm (3 bars); {11,12,13,14,15,16,17} mm (2 bars each); 18 mm (6 bars); and {18.5,19} mm (2 bars each). As reference, 4 bars were tested without any diameter reduction. The total specimen length was generally 500 mm; for small remaining diameters, it was reduced to improve machining precision (to 370 mm for diameters 16 and 17 mm and to 310 mm for smaller diameters, respectively). Constant cooling of the reinforcing bars during turning prevented heat inflow and ensured that steel microstructure and steel characteristics were not altered. The shape of all reinforcing bars was scanned before testing using an optical three-dimensional scanner (ATOS Core by GOM). This provided a very accurate measurement of the residual diameters, which differed slightly from the target values. The geometry of diameter reduction was chosen to isolate the effect of the different mechanical characteristics of the distinct microstructure layers, rather than trying to simulate the pit geometry of reinforcing bars affected by natural pitting corrosion.

When testing short specimens, it is essential to avoid the influence of bending moments due to any geometrical misalignment of the machine heads or the clamping. For this purpose, load introduction heads with spherical hinges were installed on the tensile testing machine (see Fig. 1). Specimens were connected to the load introduction heads using stiff slotted steel plates ("two-part washers"). They were loaded displacement controlled until failure at a constant strain rate of 0.1‰/s, using a LVDT of 100 mm gauge length for elongation measurement in the part with reduced diameter. Additionally, for this type of reinforcement and for comparison for a cold-worked reinforcing bar presented in [9] (referred to as CW reinforcing bar), Vickers hardness distribution over the cross section was determined on cut and grinded samples, and the microstructure was analysed after polishing and edging (Nital 3% for 5 s), using a microscope [31].

3. Results and Discussion

3.1. Microstructure analysis and Vickers hardness test

Cuts of the reinforcing bars of this test series and of a CW reinforcing bar reveal the distinct microstructure of the two types of

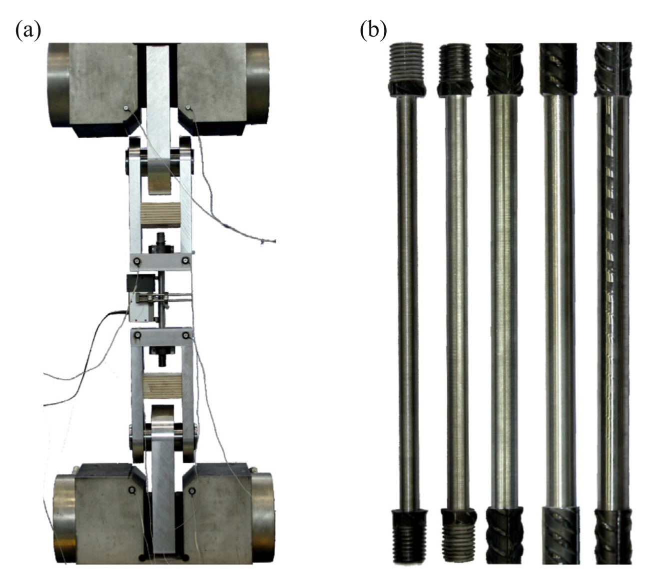

Fig. 1. (a) Heads of universal testing machine with specimen, spherical hinges and LVDT; (b) specimens with residual diameter 11, 13, 16, 18, and 18.5 mm.

reinforcing bars. Fig. 2 shows an enlargement of the surface of the different prepared cuts and photos of the corresponding samples (right lower corners). In Fig. 2(a) and (c), the various material layers of the QST reinforcing bars are visible even by eye (photos), whereas the CW reinforcing bar visually shows a homogeneous surface (Fig. 2(b)). Fig. 2(a) and (c) show enlargements of the microstructure of the QST reinforcing bar, for the central zone and for the edge zone. The edge zone exhibits needle-like crystals which are typical for martensite [31]. The central zone exhibits a structure with larger crystals, typical for a mixture of ferrite and perlite [31]. The same crystal structure is found over the whole cross section for the CW reinforcing bar, see Fig. 2(b). A Vickers hardness test performed on the QST reinforcing bar (Fig. 2(d)) exhibits a zone with almost constant hardness of 170 kgf/mm^2 up to a radii ratio r_{b1}/R = 0.65, a zone of increasing hardness up to r_{b2}/R = 0.85, followed by a zone of again fairly constant hardness of 270 kgf/mm^2. The hardness of the various zones additionally indicates the distinct material layers of the QST reinforcing bars and is consistent with the results of the microstructure analysis. A comparison of the location of the layer boundaries with literature values in Table 1 shows a good agreement. Fig. 2(d) also compares the hardness over the cross section of the QST and CW reinforcing bars, and illustrates that the CW reinforcing bar exhibits a fairly constant hardness over its cross section, confirming its uniform microstructure.

3.2. Results of tensile tests

Fig. 3(a) shows the results of the tensile tests on the specimens for varying residual diameter. Stresses are calculated using the true (as opposed to nominal) residual cross sectional area determined by laser scanning. It can be seen that the yield stress and tensile strength decrease significantly with reduced residual diameter, while the strain at peak stress exhibits a slight increase. In Fig. 3(b), the measured yield stresses and tensile strengths are plotted against the residual effective diameter d_c, confirming the higher strength with increasing (i.e., less reduced) diameter. The vertical red lines correspond to diameter ratios r/R 0.65 and 0.85, respectively (with R = 20.20 mm being the true equivalent initial bar radius, determined by laser scanning). They separate the three distinct regions determined by Vickers hardness tests. For diameters below d_c = 13.1 mm (=2x 0.65R), as well as diameters above d_c = 17.2 mm (=2x 0.85R), the tensile strength is fairly constant, with a transition zone of increasing strength between these diameters. This result substantiates the findings of the Vickers hardness tests.

To determine the mechanical characteristics of the distinct layers (annuli), the contribution of Layer j, bounded by diameters $d_{i-1} = 2r_{i-1}$ and $d_i = 2r_i$ (see Fig. 4), to the total force of the reinforcing bar is calculated at specific strain values ε using Eq. (1):

$$\sigma_j(\varepsilon) = \frac{A_i\sigma_i(\varepsilon) - A_{i-1}\sigma_{i-1}(\varepsilon)}{A_i - A_{i-1}} \quad (1)$$

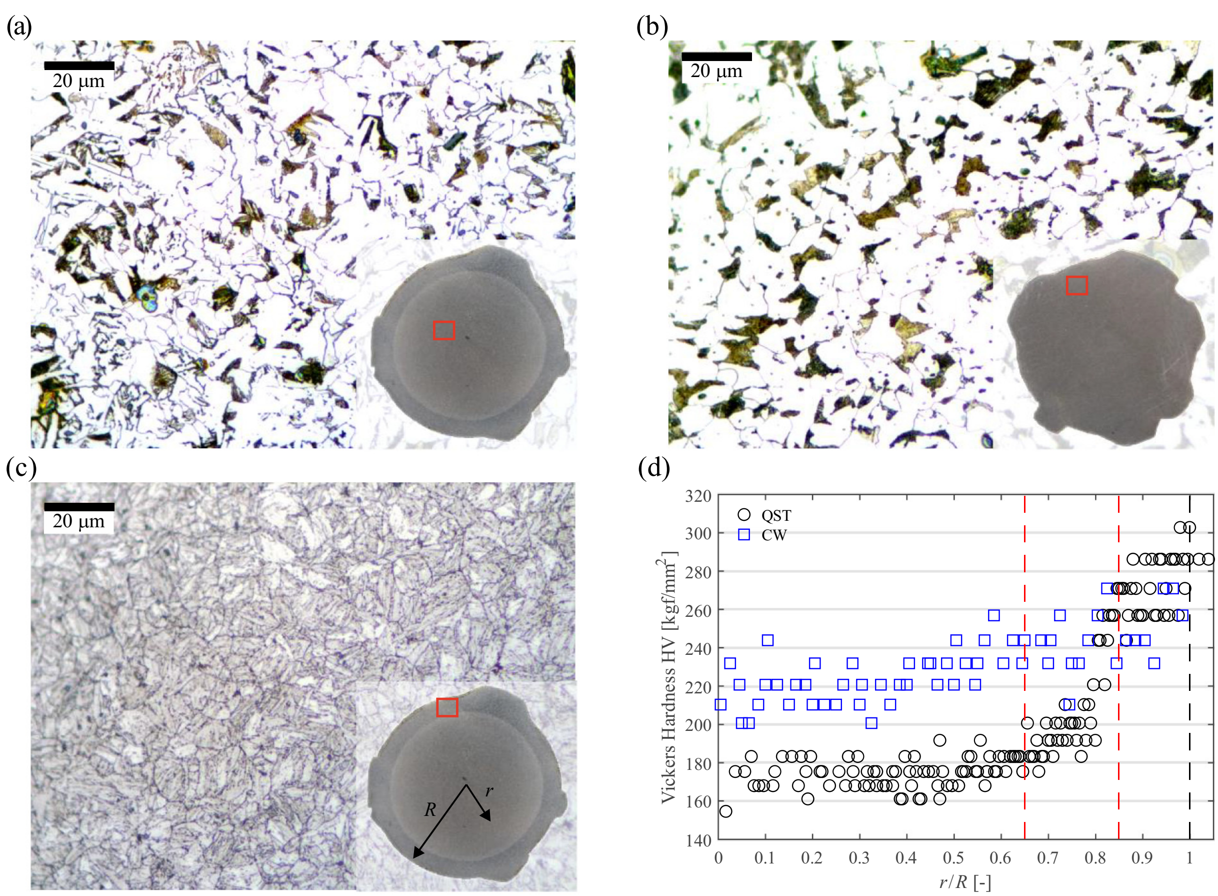

Fig. 2. (a) Microstructure in the centre of QST reinforcing bar; (b) microstructure close to edge of CW reinforcing bar; (c) microstructure close to edge of QST reinforcing bar; (d) results of Vickers hardness tests over cross section for QST and CW reinforcing bar. Red lines denote layer boundaries of core, transition zone and outer annulus of QST reinforcing bar. For r/R > 1, values correspond to the hardness of the adjacent rib. (For interpretation of the references to colour in this figure legend, the reader is referred to the web version of this article.)

Table 1
Layer boundaries between core and transition zone, and transition zone and outer annulus, obtained from Vickers hardness tests in various test series.

Researcher	Cadoni [29]	Cadoni [29]	Santos [12]	Fernandez [11]	Bautista [26]	This study
diameter $2R$ [mm]	40	32	20	12	12	20
core – transition zone r_{b1}/R [-]	0.5	0.5	0.6	0.66	0.79	0.65
transition zone – outer annulus r_{b2}/R [-]	0.85	0.8	0.8	0.92	0.88	0.85

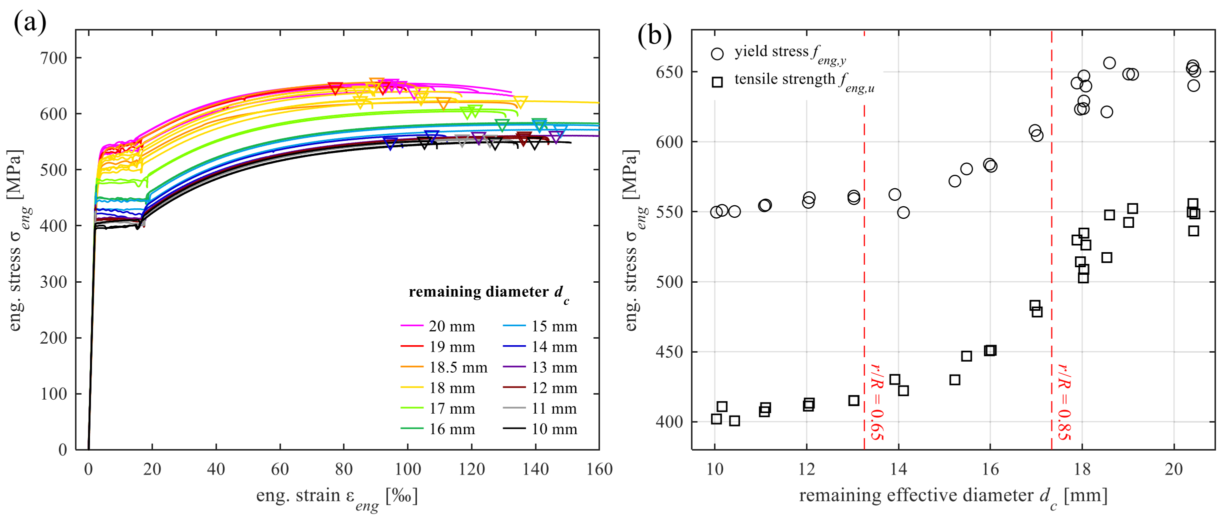

Fig 3. (a) Stress–strain diagram for specimens with varying residual diameter d_c. Triangles indicate the peak stress and corresponding strain. (b) residual effective diameter of specimens and corresponding yield stress and tensile strength. Red lines denote layer boundaries of core, transition zone and outer annulus. (For interpretation of the references to colour in this figure legend, the reader is referred to the web version of this article.)

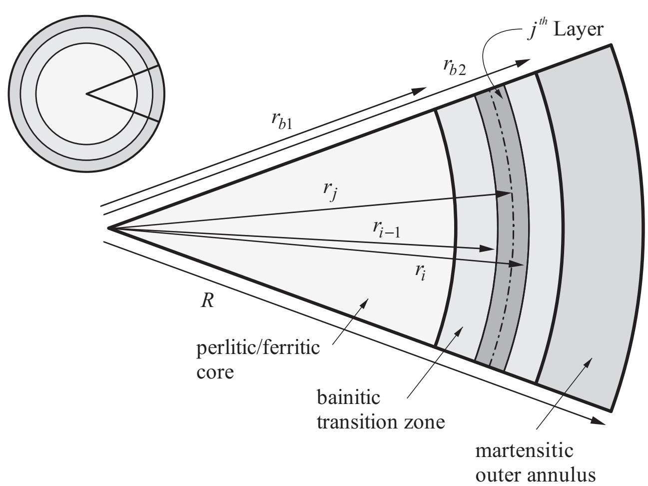

Fig. 4. Definition of variables for the calculation of the characteristics of the distinct layers.

Here, $A_i\sigma_i(\varepsilon)$ denotes the measured force at a specific strain ε for a specimen with residual effective diameter d_i, whereas $A_{i-1}\sigma_{i-1}(\varepsilon)$ denotes the measured force at the same strain ε for a specimen with the consecutive smaller diameter d_{i-1}. The difference in force is attributed to Layer j, having an area of $A_i - A_{i-1}$.

Repeating this calculation for various strain values ε and all tested diameters, one gets the stress–strain diagrams for each Layer j shown in Fig. 5(a) - (c). All layers up to diameter d_c = 13 mm exhibit essentially the same mechanical behaviour; they belong to the perlitic/ferritic core of the reinforcing bar. The results for yield stress and tensile strength match the values of the directly obtained stress-strain diagrams of the corresponding specimens, see Fig. 3(a) and (b). With increasing diameter, layers between d_c = 13 and 18 mm show an increasing yield stress and tensile strength and a decreasing strain at peak stress. The outer layers, between diameter d_c = 18 mm and the initial diameter, again exhibit a more uniform mechanical behaviour. From Fig. 5(c), it can be seen that the strains at peak stress are very similar, but the yield stress and the tensile strength in the outer layers vary more. The observed differences are presumably due to variations of the martensite content in the outermost layers: The process of a uniform mechanical reduction of the cross section is initially very demanding due to the ribs, causing uncertainty when determining the centre of the bar area. Hence, the latter may deviate from the bar axis, such that not all material that is removed is indeed part of the martensitic outer annulus. Although having the same effective diameter, these specimens thus exhibit different tensile strengths. However, the exhibited stress values of the outer annulus (between 700 and 800 MPa) are in all cases significantly higher than those of the reinforcing bar without any reduction in cross section (677 MPa, compare grey curve in Fig. 5). This corresponds to results commonly found in literature ([10,11,29]). The undamaged reinforcing bar can be interpreted as a composition of the different layers, and its stress-strain behaviour thus equals the integral of all layer characteristics, i.e. the sum of layer characteristics weighted by their corresponding areas when using discrete layers. Consequently, the martensitic outer annulus has to exhibit a strength higher than the composite bar, as the ferritic/perlitic core exhibits a strength lower than the one of the composite bar.

Comparing the stress-strain diagrams in Fig. 5, one observes that a pronounced yield plateau exists for the ferritic/perlitic core and the transition zone up to d_c = 17 mm, whereas the martensitic outer annulus shows a behaviour similar to hot-rolled and cold-stretched reinforcing bars with gradual transition to hardening at the end of the elastic phase, lacking a yield plateau.

A substantial difference in the strain at peak stress is visible when comparing the results of the martensitic layer (Fig. 5(c),

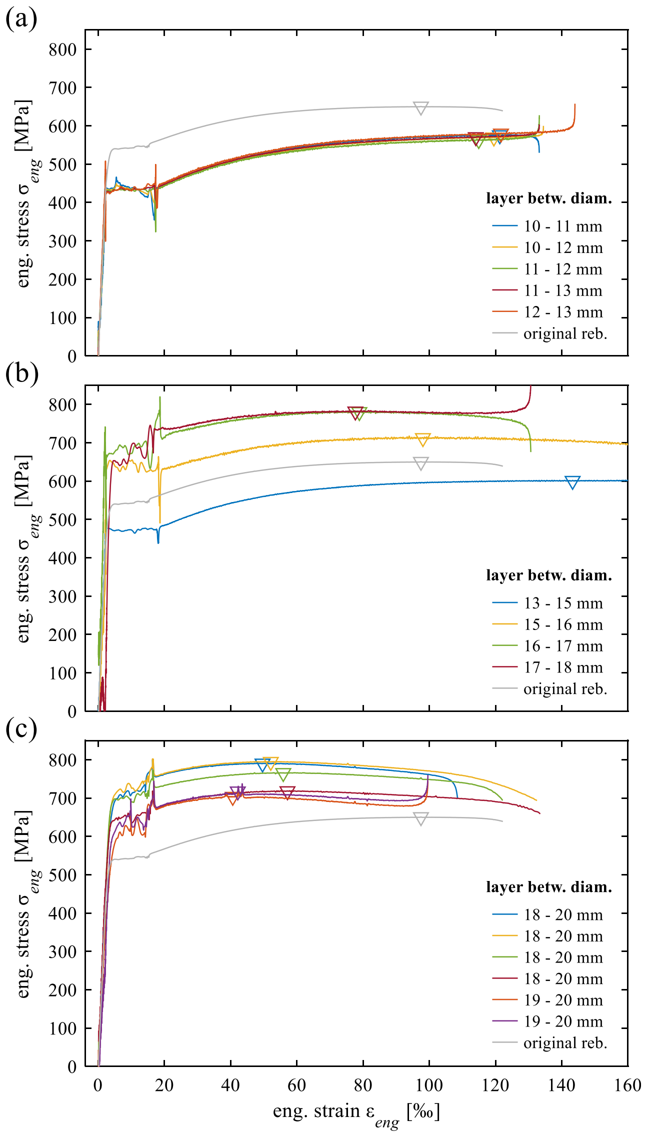

Fig. 5. Calculated stress–strain diagrams for (a) core, (b) transition zone and (c) outer annulus. Triangles indicate peak stress and corresponding strain. In grey, the curve of an original reinforcing bar of the same batch is shown for comparison.

$\varepsilon_{eng,mart}(f_{eng,u}) \approx 60‰$) and those of the undamaged reinforcing bar (Fig. 5(c), grey line, $\varepsilon_{eng,tot}(f_{eng,u}) \approx 100‰$). In the engineering stress - engineering strain diagram – as commonly used in structural engineering –, this point marks the end of uniform elongation in a tensile test, i.e., the beginning of necking in the failure zone, and corresponds to the tensile strength of the specimen, since engineering stresses are related to the initial, constant area. Nevertheless, the material itself undergoes much higher stresses in the necking phase if the true area $A(\varepsilon)$ is considered [32]. If strain compatibility without slip between layers is postulated for the entire reinforcing bar during a tensile test, true strains are equal across any cross section and consequently, the martensitic layer is stretched beyond its strain at peak engineering stress. As in the experiments neither cracks on the specimens' surface nor local necking were observed, it is highly probable that at strains beyond $\varepsilon_{eng,mart}(f_{eng,u})$, the area of the martensitic layer – supported by the ferritic/perlitic core – was reduced uniformly, leading to an increase in true stress. As soon as the tensile strength of the ferritic/perlitic core is reached at higher strains, necking over the entire cross section occurred at the weakest point along the reinforcing bar, leading to a failure of the whole reinforcing bar. Hortigón Fuentes et al. [10] independently set up the same hypothesis, supported by experimental indications obtained from metallographic measurements of the thicknesses of core and outer annulus.

Fig. 6(a) shows the true stress - true strain diagram for the layers between diameter d_c 18 and 20 mm (similar to Fig. 5(c), where conventional engineering stresses and strains were used). The general shape of the curve is not altered, but the strain at peak stress increases substantially (compare grey lines in Fig. 6(a)). The conversion from engineering to true stresses and strains was carried out using the relationships:

$$\varepsilon_{tr} = \ln(1+\varepsilon_{eng}) \tag{2}$$

$$\sigma_{tr} = (1+\varepsilon_{eng})\sigma_{eng} \tag{3}$$

where Eq. (2) can be derived by solving the differential equation of the true strains $d\varepsilon_{tr} = dl/l$ [32], and Eq. (3) follows from the assumption of constant volume [32]. Hence, these equations apply only as long as no local necking (which involves the formation of voids) occurs, i.e., for $\varepsilon_{tr,\max} \leqslant \ln(1+\varepsilon_{eng,tot}(f_{eng,u})) \approx \ln(1+0.1) = 0.095$, with $\varepsilon_{eng,tot}(f_{eng,u})$ = strain at peak stress of the undamaged reinforcing bar in engineering values. This value is reached shortly after passing the maximum true stress in Fig. 6(a).

Fig. 6(b) compares the true strains corresponding to the true tensile strength of the distinct layers (calculated values) to the results of the tensile tests (measured values). It can be seen that for the martensitic outer annulus between diameter d_c 18 and 20 mm, true strains closely match the true strains of the composite reinforcing bar. This result supports the hypothesis that the martensitic outer annulus is strained above its strain at peak stress determined from the engineering stress-strain diagram, as outlined in the previous section. Since the elongation beyond peak engineering stress of the outer annulus is controlled by the more ductile perlitic/ferritic core, its true strains at peak true stress have to be higher than in engineering values, which represent the behaviour of the material without the support of the core (and for which the true strains at peak true stress are always smaller than in engineering values, see Eq. (2)).

3.3. Constitutive models for ferritic/perlitic core and martensitic outer annulus

In the following, constitutive relationships for the perlitic/ferritic core and the martensitic outer annulus are proposed, that will subsequently be used to model the stress-strain behaviour of the entire reinforcing bar composed of these two materials and bainite. Note that the basic characteristics (yield stress, tensile strength and corresponding strains at yielding, onset of hardening and tensile strength, respectively) have to be determined based on the true stress-true strain diagrams. They cannot be directly back calculated from the values obtained using engineering stress-strain diagrams as outlined below. However, once the basic values have been obtained from the stress-strain diagram in true values, they can be converted back to their equivalent points in engineering values using Eqs. (2) and (3).

The following equations are used to define the constitutive relationships for the perlitic/ferritic core (see Fig. 7 for notation):

$$\text{elastic phase, i.e. } 0 \leqslant \varepsilon_{tr} \leqslant \varepsilon_{tr,y} = ln\left(\frac{1+\sqrt{1+4f_{tr,y}/E}}{2}\right): \quad \sigma_{tr} = E\varepsilon_{eng}(1+\varepsilon_{eng}) = Ee^{\varepsilon_{tr}}(e^{\varepsilon_{tr}}-1) \tag{4}$$

$$\text{yielding, i.e. } \varepsilon_{tr,y} \leqslant \varepsilon_{tr} \leqslant \varepsilon_{tr,h}: \quad \sigma_{tr} = f_{tr,y}\frac{e^{\varepsilon_{tr}}}{e^{\varepsilon_{tr,y}}} = E(e^{\varepsilon_{tr,y}}-1)e^{\varepsilon_{tr}} \tag{5}$$

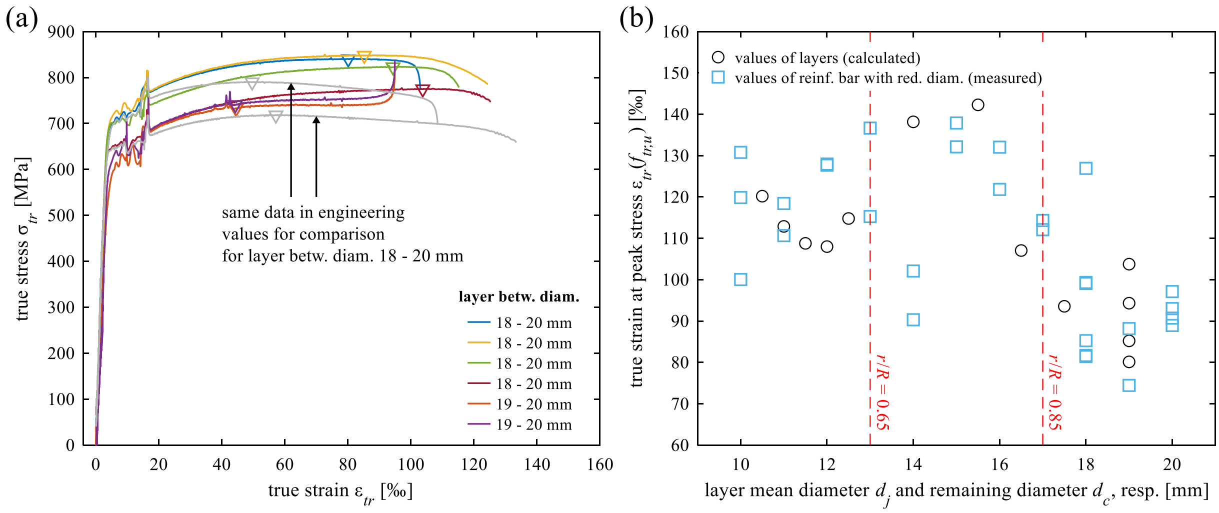

Fig 6. (a) Response of outer annulus in true stress and strain. Triangles indicate peak stress and corresponding strain. (b) Calculated true strain at true tensile strength for different layers with 1 mm thickness depending on their position (mean diameter $d_j = 2r_j$ acc. to Fig. 4) and results of tensile tests for specimens with corresponding residual diameter d_c.

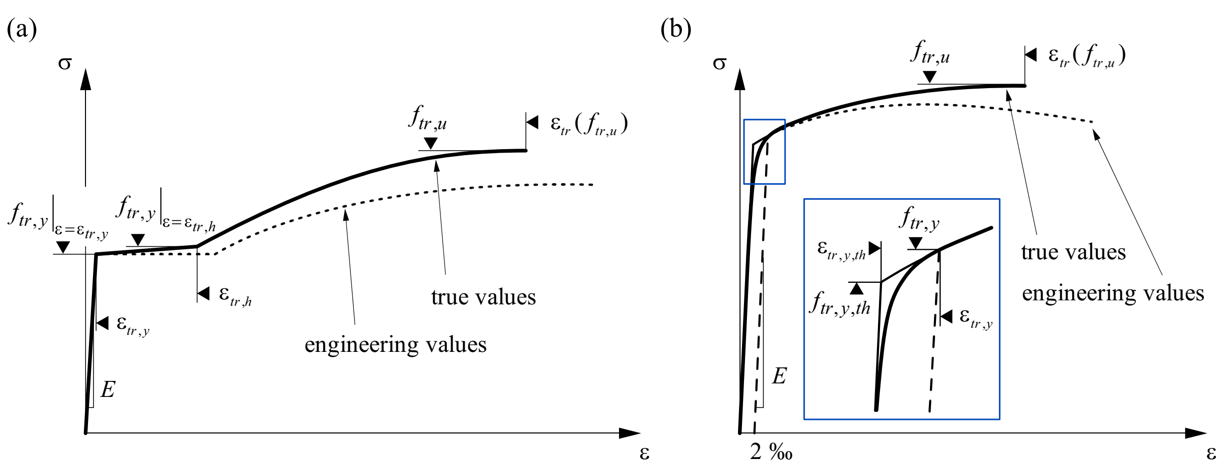

Fig. 7. Definition of material characteristics for the constitutive relationships (a) of the perlitic/ferritic core; (b) of the martensitic outer annulus.

$$\text{hardening, i.e. } \varepsilon_{tr,h} \leqslant \varepsilon_{tr} \leqslant \varepsilon_{tr}(f_{tr,u}):$$
$$\sigma_{tr} = e^{\varepsilon_{tr}}\left[\frac{f_{tr,u}}{e^{\varepsilon_{tr}(f_{tr,u})}} - \left(\frac{f_{tr,u}}{e^{\varepsilon_{tr}(f_{tr,u})}} - \frac{f_{tr,y}|_{\varepsilon_{tr}=\varepsilon_{tr,y}}}{e^{\varepsilon_{tr,y}}}\right)\left(\frac{e^{\varepsilon_{tr}(f_{tr,u})} - e^{\varepsilon_{tr}}}{e^{\varepsilon_{tr}(f_{tr,u})} - e^{\varepsilon_{tr,h}}}\right)^{\beta}\right] \tag{6}$$

In Eq. (6) (and Eq. (8) below), β is a model coefficient whose value is determined by regression of the experimental data in true values. Table 2 summarises the values of the material characteristics in true values, as determined in our test series.

The constitutive relationships for the martensitic outer annulus are defined as follows:

$$\text{elastic phase, i.e. } 0 \leqslant \varepsilon_{tr} \leqslant \varepsilon_{tr,y,th}:$$
$$\sigma_{tr} = E\varepsilon_{eng}(1 + \varepsilon_{eng}) = Ee^{\varepsilon_{tr}}(e^{\varepsilon_{tr}} - 1) \tag{7}$$

$$\text{hardening, i.e. } \varepsilon_{tr,y,th} \leqslant \varepsilon_{tr} \leqslant \varepsilon_{tr}(f_{tr,u}):$$
$$\sigma_{tr} = f_{tr,u} - (f_{tr,u} - f_{tr,y})\left(\frac{\varepsilon_{tr}(f_{tr,u}) - \varepsilon_{tr}}{\varepsilon_{tr}(f_{tr,u}) - \varepsilon_{tr,y}}\right)^{\beta} \tag{8}$$

Fig. 8 shows the stress-strain curves for each layer back calculated from experiments (in grey) and the model curves based on the Eqs. (4)-(8) for the perlitic/ferritic core and the martensitic outer annulus in engineering (a) and true values (b). The models closely capture the shape of the experimental curves, despite that they contain merely one single fitting parameter (the exponent β). This is particularly noteworthy for the part with negative slope of the martensitic outer annulus in Fig. 8(a), at strains beyond the engineering tensile strength, which is obtained directly from the model (expressed in true values and transformed into engineering values) by simply inserting the basic characteristics obtained from the experimentally observed true stress-strain diagram. Fig. 8 nicely demonstrates that for the martensitic outer annulus, the tensile strength (and corresponding strain) determined from true values differs significantly from the tensile strength (and the corresponding strain) obtained directly in engineering values. Hence, the proper failure point of the material can only be captured correctly from the true stress-strain diagram.

3.4. Proposed model for a composed QST reinforcing bar

Based on the two constitutive relationships (Eq. (4)-(8)), the stress-strain behaviour of a reinforcing bar composed of a perlitic/ferritic core, a banitic transition zone and a martensitic outer annulus is obtained by integration over the cross section. The resulting model allows to describe the behaviour of QST reinforcing bars with intact or reduced cross section. While all calculations have

Table 2
Material characteristics of perlitic/ferritic core, martensitic outer annulus, and composed original reinforcing bar as determined in the experiments. Stresses and strains are given in true values.

		Core	Outer annulus	Composed rebar
E_s	[GPa]	205	205	205
$\varepsilon_{tr,y}$	[-]	0.002	0.0055	0.0047
$\varepsilon_{tr,y,th}$	[-]	–	0.0034	–
$\varepsilon_{tr,h}$	[-]	0.017	–	0.016
$\varepsilon_{tr}(f_{tr,u})$	[-]	0.121	0.092	0.0969
$f_{tr,y}\vert_{\varepsilon_{tr}=\varepsilon_{tr,y}}$	[MPa]	410	707	542
$f_{tr,y}\vert_{\varepsilon_{tr}=\varepsilon_{tr,h}}$	[MPa]	416	–	563
$f_{tr,u}$	[MPa]	627	852	712
β	[-]	2.94	3.4	–

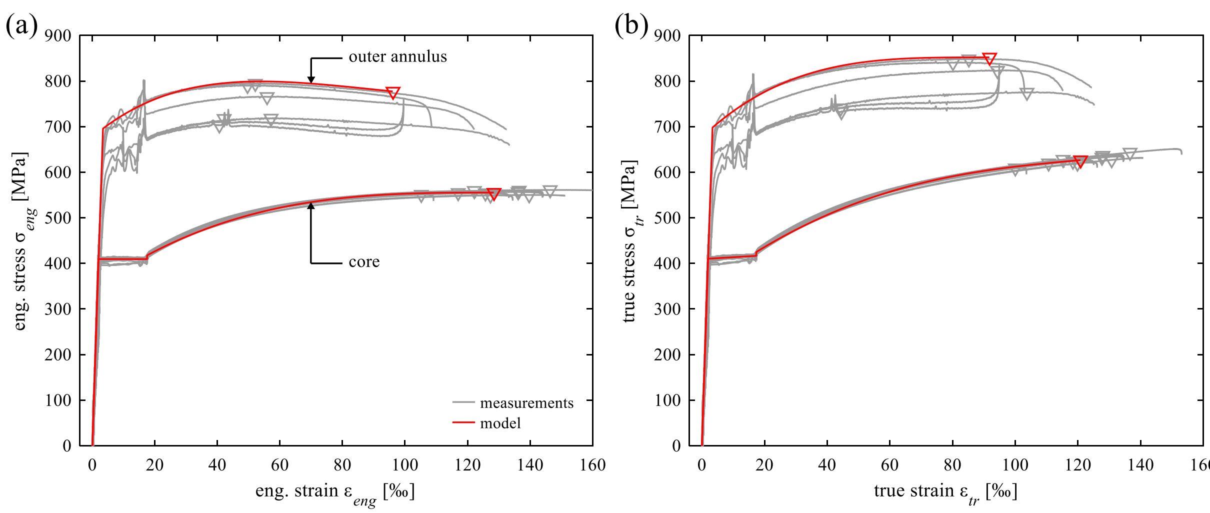

Fig 8. Stress–strain diagram of perlitic/ferritic core and martensitic outer annulus back calculated from experiments in grey, and constitutive material model in red in (a) engineering and (b) true values. Triangles denote is the peak stress in the experimental curves and maximum true stress in the model curves (resp. its equivalent in engineering values), and the corresponding strains. (For interpretation of the references to colour in this figure legend, the reader is referred to the web version of this article.)

to be carried out using true stress-strain values, the results can finally be converted to engineering values.

The numerical model is based on the following principles and the notation shown in Figs. 4 and 7:

1. Determine r_{b1} and r_{b2} denoting the border of the core and the transition zone.
2. Obtain the constitutive relationships for perlite/ferrite and martensite (Eqs. (4)-(8)).
3. Determine constitutive relationship of bainitic transition zone, using the relationship derived for perlite/ferrite (Eqs. (4)-(6)), but assuming a linear variation of yield stress and tensile strength from ferrite/perlite at $r = r_{b1}$ to martensite at $r = r_{b2}$:

$$\begin{aligned} &\text{for } r_{b1} < r \leqslant r_{b2} : f_{tr,y,bain}(r) = \left(f_{tr,y,mart} - f_{tr,y,core}\right)(r - r_{b1})/(r_{b2} - r_{b1}) \\ &\quad + f_{tr,y,core} f_{tr,u,bain}(r) = \left(f_{tr,u,mart} - f_{tr,u,core}\right)(r - r_{b1})/(r_{b2} - r_{b1}) \\ &\quad + f_{tr,u,core}\ \varepsilon_{tr,y,bain} = f_{tr,y,bain}/E \varepsilon_{tr,h,bain} = \varepsilon_{tr,h,core} \\ &\quad\ \varepsilon_{tr,bain}(f_{tr,u}) = \varepsilon_{tr,core}(f_{tr,u}) E = 205\ \text{GPa} \beta = 3.8 \end{aligned} \tag{9}$$

4. Calculate sum of stresses in all layers for a specific strain value ε, weighted by their area A in the cross section with total area A_{tot}:

$$\sigma_{tr,tot}(\varepsilon_{tr}) = \frac{A_{core}}{A_{tot}} \sigma_{tr,core}(\varepsilon_{tr}) + \sum_j \frac{A_{bain}(r_j)}{A_{tot}} \sigma_{tr,bain}(r_j, \varepsilon_{tr}) + \frac{A_{mart}}{A_{tot}} \sigma_{tr,mart}(\varepsilon_{tr}) \tag{10}$$

Note that the contribution of the bainitic transition zone is nonlinear, as the strength of the bainite is linear in r, and the total bainitic area is quadratic in r. To determine the behaviour of a reinforcing bar with non-axisymmetrically reduced cross section, the area of the damaged zone can be discretised over r and the weighted stresses of each element summed up. In the special case of a uniform, all-sided reduction of the cross section, Eq. (10) can be simplified and discretisation avoided. With $\tilde{r}$ denoting the outermost radius of the (remaining) bainitic transition zone ($r_{b1} < \tilde{r} \leqslant r_{b2}$) and $\alpha = \tilde{r}/r_{b1}$ the ratio of radii, integration of the total yield load and tensile resistance of the transition zone yields: $F_{tr,y,bain}\left(\tilde{r}\right) = \int_{r_{b1}}^{\tilde{r}} 2r\pi f_{tr,y,bain}(r)dr = \frac{\pi r_{b1}^3}{3(r_{b2}-r_{b1})}(\alpha - 1)^2(2\alpha + 1) \left(f_{tr,y,mart} - f_{tr,y,core}\right) + (\alpha^2 - 1)\pi r_{b1}^2 f_{tr,y,core} F_{tr,u,bain}\left(\tilde{r}\right) = \int_{r_{b1}}^{\tilde{r}} 2r\pi f_{tr,u,bain}(r)dr = \frac{\pi r_{b1}^3}{3(r_{b2}-r_{b1})}(\alpha - 1)^2(2\alpha + 1)\left(f_{tr,u,mart} - f_{tr,u,core}\right) + (\alpha^2 - 1)\pi r_{b1}^2 f_{tr,u,core}$

Dividing by the total area of the transition zone $A_{bain}\left(\tilde{r}\right) = \int_{r_{b1}}^{\tilde{r}} 2r\pi dr = \pi\left(\tilde{r}^2 - r_{b1}^2\right) = (\alpha^2 - 1)\pi r_{b1}^2$ one gets the mean yield stress and tensile strength, $\bar{f}_{tr,y,bain}\left(\tilde{r}\right)$ and $\bar{f}_{tr,u,bain}\left(\tilde{r}\right)$, respectively:

$$\begin{aligned} \bar{f}_{tr,y,bain}\left(\tilde{r}\right) &= F_{tr,y,bain}\left(\tilde{r}\right)/A_{bain}\left(\tilde{r}\right) = \frac{\pi r_{b1}}{3(r_{b2}-r_{b1})} \frac{(\alpha-1)(2\alpha+1)}{(\alpha+1)} \left(f_{tr,y,mart} - f_{tr,y,core}\right) + f_{tr,y,core} \\ \bar{f}_{tr,u,bain}\left(\tilde{r}\right) &= F_{tr,u,bain}\left(\tilde{r}\right)/A_{bain}\left(\tilde{r}\right) = \frac{\pi r_{b1}}{3(r_{b2}-r_{b1})} \frac{(\alpha-1)(2\alpha+1)}{(\alpha+1)} \left(f_{tr,u,mart} - f_{tr,u,core}\right) + f_{tr,u,core} \end{aligned} \tag{11}$$

Yield stress and tensile strength, $f_{tr,y,bain}(r)$ and $f_{tr,u,bain}(r)$, can then be substituted in Eq. (9) by their mean values (Eq. (11)), and the constitutive model for bainite be written accordingly, resulting in an average stress in the bainitic transition zone $\bar{\sigma}_{tr,bain}\left(\tilde{r}, \varepsilon_{tr}\right)$ independent of the discretised radius r. The second term of the sum in Eq. (10) can thus be rewritten as: $\sum_j \frac{A_{bain}(r_j)}{A_{tot}} \sigma_{tr,bain}(r_j, \varepsilon_{tr}) = \frac{A_{bain}(\tilde{r})}{A_{tot}} \bar{\sigma}_{tr,bain}\left(\tilde{r}, \varepsilon_{tr}\right)$.

After having developed the model outlined above, the authors became aware of a publication of Hortigón Fuentes et al. [10], who presented a similar approach for modelling the stress-strain behaviour of a reinforcing bar by summing up weighted true stresses in concentric layers. However, they considered only two zones with distinct thicknesses and material characteristics, and their model, requiring finite element calculations to obtain the behaviour of the composite reinforcing bar, neither captures reinforcing bar rupture nor the behaviour of damaged zones. These issues are overcome with the approach proposed here, which considers all three relevant zones of an intact or damaged QST reinforcing bar and can easily be implemented in a simple spreadsheet. Nevertheless, the similarity of both independently developed models and their good correlation with experimental data show their potential and confirm the underlying hypotheses.

3.5. Comparison of proposed model with experimental data

Fig. 9(a) compares the experimental curves with the calculations of the model proposed in Section 3.4. Calculations were done in true stress-strain values and the results transformed to engineering values. Model predictions and experimental data are in almost perfect agreement.

The observed behaviour at the transition from the elastic phase to yielding (compare the zoomed-in region in Fig. 9(b)) merits a closer look and discussion: A distinct upper yield point with subsequent serrated flow at a fairly constant average stress was clearly observed for the perlitic/ferritic core and the bainitic transition zone. As documented in literature [32–34], this is typical for the plastic flow of metals with dissolved atoms of sufficient diffusivity (e.g. interstitial carbon atoms in ferritic steel) in a displacement controlled tensile test. Without applied stress, the interstitial atoms diffuse to the metal's defects at atomic level, known as dislocations, and subsequently impede movements along gliding planes at low applied stresses. Once the applied stresses exceed the upper yield point, dislocations can break free and move freely, causing an immediate drop of the stress to the lower yield point. This process starts in a small number of crystalline grains with optimally oriented gliding planes, where local deformations build up. Dislocations then accumulate at the boundaries to the adjoining grains and stress increases again, until the dislocations of the adjacent grain break free, leading to a cascaded formation of strain localisations known as Lüders bands. The process continues at variable stress – between upper and lower yield point – until all dislocations are unpinned and able to move. At this point, the yielding phase ends, i.e., the end of the yield plateau in the stress-strain diagram has been reached, and the phase of strain hardening begins subsequently.

If the composed reinforcing bar includes a martensitic outer annulus, the observed behaviour changes markedly. Rather than exhibiting a distinct upper yield point, the slope of the stress-strain curve decreases gradually, and the stress clearly increases during the yielding phase with increasing strain. This change in behaviour can be explained by the fact, that the stress-strain curve of the martensitic outer annulus does not exhibit any yield plateau when reaching the yield stress. Instead, strain hardening in the martensitic layer immediately follows the elastic phase. Furthermore, the yield stress for martensite is almost twice as high as the yield point of the perlitic/ferritic core ($f_{eng,y,mart}$ = 706 MPa $\gg$ $f_{eng,y,core}$ = 409 MPa in the used samples). Consequently, the stress-strain curve of the composite reinforcing bar becomes flatter at 409 MPa (core is yielding, outer annulus is still elastic). Once the end of the elastic phase of the outer annulus is reached (706 MPa for the martensitic outer annulus or 548 MPa on average of the composed material), the curve flattens again. In the following phase, stresses increase since the martensitic outer annulus strain hardens, whereas the perlitic/ferritic core and the bainitic transition zone yield at constant stress. At the end of the yield plateau of core and transition zone, these layers start strain hardening, causing the stress-strain curve of the composite bar to become markedly steeper again. The proposed model represents these phenomena very well.

3.6. Influence of microstructure on the residual tensile strength of a corroded reinforcing bar

Fig. 10 compares the remaining tensile resistance of a unilaterally and uniformly damaged QST reinforcing bar for a given loss of cross sectional area $\zeta = A_{lost}/A_{tot}$ (a) to the tensile resistance of an original reinforcing bar; and (b) to the residual tensile resistance of a cold-worked CW reinforcing bar with the same initial strength and equal damage. Whereas due to its homogeneous composition, the residual strength of the CW reinforcing bar is directly proportional to the loss of cross section, the uniformly damaged QST reinforcing bar reveals a disproportionate loss of strength. This behaviour directly results from the loss of the martensitic and bainitc layers, which are responsible for the high strength of a QST

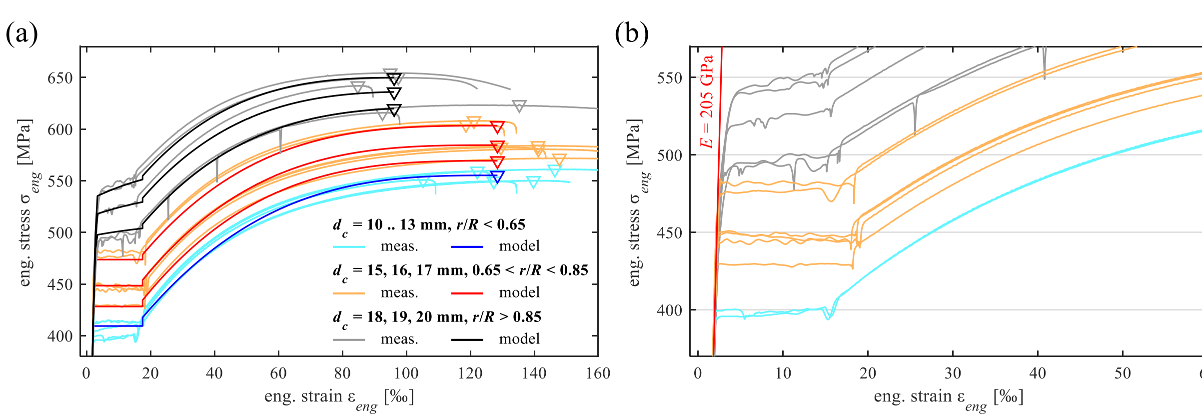

Fig. 9. (a) Comparison of model and experimental curves of reinforcing bars with uniformly reduced diameter d_c; (b) zoomed-in region between yielding and hardening of selected experimental curves.

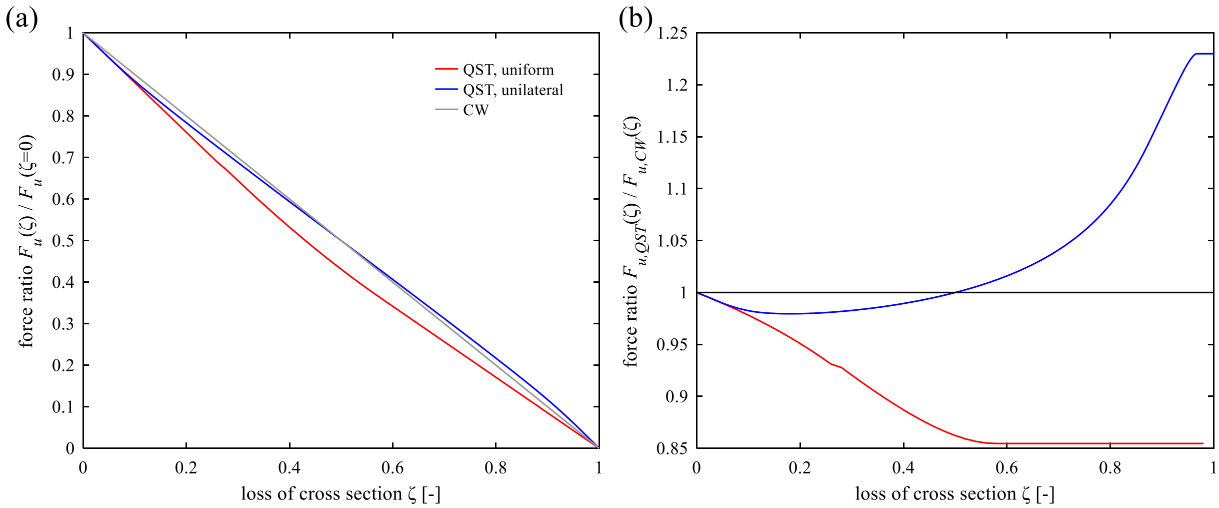

Fig. 10. (a) Remaining tensile resistance of a uniformly damaged QST, a unilaterally damaged QST, and a cold-worked CW reinforcing bar as function of the cross section loss, compared to the tensile resistance of an original reinforcing bar; (b) Ratio of remaining tensile resistance of a uniformly and a unilaterally damaged QST reinforcing bar compared to a CW reinforcing bar with the same initial strength and equal damage as function of the cross section loss.

reinforcing bar. At a residual cross sectional area of 43% of the original area (ζ = 0.57), only the perlitic/ferritic core remains, having a markedly lower strength than the composite material. With further degradation beyond this point, the residual force ratio between the QST and the CW reinforcing bar remains constant (slightly above 0.85, compare Fig. 10(b)).

A unilaterally damaged QST reinforcing bar also exhibits a disproportionate strength degradation up to a cross section loss of 50%, but much less drastically than the uniformly damaged bar (minimum strength ratio of 0.98 between a QST and a CW bar at ζ = 0.2). This is due to an approximately even removal of martensitic and perlitic/ferritic material. For cross section losses higher than 50%, the strength ratio between a QST and an equally damaged CW reinforcing bar is even higher than 1, as the area of the martensitic layer prevails.

The findings of Fig. 10 highlight that depending on the damage geometry, QST reinforcing bars can disproportionally lose strength if the martensitic layer is lost. Especially for uniformly corroded reinforcing bars, this effect has to be taken into account when assessing the structural safety. In contrast, unilaterally damaged QST reinforcing bars do not lose more strength than equally damaged CW reinforcing bars. This is of high practical relevance, as chloride induced corrosion leads in the majority of cases to a unilateral damage of reinforcing bars. However, it has to be noted that with a severe unilateral damage, other effects occur, such as local bending moments, which may significantly affect the bearing capacity of the reinforcing bar [15,16,23,25].

3.7. Estimation of model parameters for predicting the strength of damaged QST reinforcing bars

In the validation above, the results of the model match the experimental curves very well since the input values (yield stress and tensile strength and corresponding strains) could be obtained from the tensile tests. Obviously, carrying out such as an expensive experimental campaign to determine these input values for a practical case, where e.g. the stress-strain characteristics of corroded reinforcing bars in an existing structure should be assessed, can hardly be justified. Therefore, a simplified approach to calculate the strength of a damaged composite rebar based on the results of conventional tensile tests is proposed, distinguishing three levels of approximation. In all of them, the ratios

$$f_{eng,u,core}/f_{eng,y,core} = 1.36 f_{eng,u,mart}/f_{eng,y,mart} = 1.10 \quad (12)$$

between tensile strength and yield stress, as observed in this study, are used. Furthermore, for simplicity, it is assumed that the composite reinforcing bars consists of only two layers, i.e. a ferritic/perlitic core and a martensitic outer annulus; the area of the bainitic layer in between is assigned equally to core and outer annulus. This simplification can be justified as follows: The tensile strength of the composed reinforcing bar is made up – according to the above simplification – proportionally by the tensile strength of core and outer annulus, i.e. $a \cdot f_{eng,u,core} + (1-a) \cdot f_{eng,u,mart} = f_{eng,u,tot}$ where a denotes a proportionality factor, which is equal to $a = 0.58$ for the tensile strength of the tested specimens. On the other hand, the weighted area of the core and half of the adjacent bainitic zone, i.e. $b = \frac{A_{core}+A_{bain}/2}{A_{tot}}$ equals $b = 0.57 \approx a$ for the tested specimens. Hence, the simplification introduced above will yield reasonable results.

3.7.1. First level of approximation

1. Determine the tensile strength $f_{eng,u,tot}$ and the yield stress $f_{eng,y,tot}$ of the composite reinforcing bar from a conventional tensile test.

2. Assume that the true strain corresponding to the tensile strength of the martensitic layer coincides with the true strain corresponding to the tensile strength of the composite bar, i.e. $\varepsilon_{tr,mart}(f_{tr,u}) = \varepsilon_{tr,tot}(f_{tr,u})$. Assume – as observed in the present test series – the true strain at peak stress of the perlitic/ferritic core to be 7% larger than the true strain at peak stress of the composite bar, i.e.:

$$\varepsilon_{tr,core}(f_{tr,u}) = 1.07 \ln(1 + \varepsilon_{eng,tot}(f_{eng,u})) \quad (13)$$

The true strain at hardening of the core can be obtained from the engineering strain at hardening of the composite bar, i.e., $\varepsilon_{tr,h,core} = \ln(1 + \varepsilon_{eng,h,tot})$.

3. Assume that the relative area of the simplified core is $\tilde{A}_{core} = b = 0.57$ (as observed in the experiments, see above) and the relative area of the simplified outer annulus is $\tilde{A}_{mart} = 1 - b = 0.43$.

4. Using Eq. (12), determine the yield stress and the tensile strength of the ferritic/perlitic core, $f_{eng,y,core}$ and $f_{eng,u,core}$, and of the martensitic layer, $f_{eng,y,mart}$ and $f_{eng,u,mart}$, respectively, by solving the following linear system of equations:

$$
\begin{aligned}
f_{eng,y,tot} &= \widetilde{A}_{core} \cdot f_{eng,y,core} + \widetilde{A}_{mart} \cdot f_{eng,y,mart} \\
f_{eng,u,tot} &= \widetilde{A}_{core} \cdot f_{eng,u,core} + \widetilde{A}_{mart} \cdot f_{eng,u,mart}
\end{aligned}
\tag{14}
$$

Alternatively, the yield stress of the core material $f_{eng,y,core}$ could also be estimated using the stress–strain diagram of the composite reinforcing bar, as it coincides with the point where the elastic region ends and the curve begins to flatten (compare Fig. 9(b)). This observation may be used to verify the appropriateness of the assumptions and simplifications made.

5. The true values of the yield stress and the tensile strength can be calculated using Eq. (2) and (3), i.e.: $f_{tr,y,core} = f_{eng,y,core} e^{\varepsilon_{tr,y,core}}$ $f_{tr,y,mart} = f_{eng,y,mart} e^{\varepsilon_{tr,y,mart}}$ $f_{tr,u,core} = f_{eng,u,core} e^{\varepsilon_{tr,core}(f_{tr,u})}$ $f_{tr,u,mart} = f_{eng,u,mart} e^{\varepsilon_{tr,mart}(f_{tr,u})}$

3.7.2. Second level of approximation

The values of the yield stress and the tensile strength of the core material, $f_{eng,y,core}$ and $f_{eng,u,core}$, respectively, are obtained by carrying out additional tensile tests on reinforcing bars with sufficiently reduced cross section to eliminate the transition zone (e.g. 50% reduction in diameter) over a length of about 10 times the original diameter. With these values, the assumption of the strength ratios (Eq. 12) can be avoided, which will improve the approximation for the yield and tensile strength of the outer annulus obtained from Eq. (14). Additionally, the true strain at peak stress of the core can be set to its experimentally determined value, rather than approximating it using Eq. (13).

3.7.3. Third level of approximation

Performing a Vickers Hardness test over the cross section of the sample, the relative areas of the core and the outer annulus, $\widetilde{A}_{core}$ and $\widetilde{A}_{mart}$, respectively, are obtained. Using this information, combined with the results of the tensile tests on the reinforcing bar with reduced diameter, the yield stress and the tensile strength of the martensitic outer annulus $f_{eng,y,mart}$ and $f_{eng,u,mart}$ can be determined with good accuracy.

4. Conclusions

This study investigated the influence of the steel microstructure on the stress-strain behaviour of hot-rolled, quenched and self-tempered (QST) reinforcing bars. As documented in literature, three distinct material layers could be identified: A ferritic/perlitic core, a bainitic transition zone and a martensitic outer annulus. Thicknesses of the distinct material layers, determined by Vickers hardness tests, were found to closely correspond to values found in literature. Tensile tests on QST reinforcing bars with gradually reduced diameters were used to reveal the stress-strain behaviour of the different microstructure layers. Constitutive relationships for the ferritic/perlitic core, the bainitc transition zone and the martensitic outer annulus were shown, together with experimental stress-strain diagrams. Experimental results confirmed that models composing a reinforcing bar out of its distinct layers cannot be formulated in conventional engineering stress and strain, but true stress and true strain must be used. A simplified model to predict the stress–strain behaviour of a QST reinforcing bar based on the constitutive relationships of its layers was proposed and validated against the experimental results, revealing excellent agreement. Finally, three levels of approximation were suggested to determine the strength of damaged QST reinforcing bars if no detailed information is available.

Knowledge about the stress-strain behaviour of the distinct layers of QST reinforcing bars and their interaction is crucial to assess the residual strength and ductility of concrete structures affected by reinforcement corrosion. Experiments and calculations reveal that the strength of uniformly damaged QST reinforcing bars is reduced up to 15% more than what would be expected if merely the loss of cross section were considered, since the inner core has much lower strength than the outer layers. In combination with the loss of cross section area, the strength is thus disproportionately reduced. On the other hand, if QST reinforcing bars are damaged unilaterally, the direct tensile strength does not alter significantly. Therefore, the different stress-strain behaviour of the distinct microstructure layers only have a minor influence in case of pitting corrosion, as this corrosion type leads in the majority of cases to a unilateral damage of reinforcing bars. However, other effects resulting from the pit geometry, such as bending due to a shift of the neutral axis, may strongly affect the bearing capacity [15,16].

The findings of this study related to the influence of microstructure on the stress-strain behaviour of corroded reinforcing bars are a first important step towards a better understanding of the structural response of concrete structures affected by reinforcement corrosion. Nonetheless, further effects need to be considered, such as e.g. the strain rate dependent strength of reinforcing bars [9], three-dimensional stress states in the vicinity of localised corrosion pits, or bending moments in case of a unilateral damage. The authors are currently investigating these additional effects, in order to finally be able to accurately assess the residual safety of corroded reinforced concrete structures.

CRediT authorship contribution statement

Severin Haefliger: Conceptualization, Methodology, Software, Investigation, Writing - original draft, Visualization. **Walter Kaufmann:** Conceptualization, Methodology, Writing - review & editing, Supervision, Funding acquisition.

Declaration of Competing Interest

The authors declare that they have no known competing financial interests or personal relationships that could have appeared to influence the work reported in this paper.

Acknowledgements

The experiments of this study were carried out as a part of the Master's Thesis of Sara Fomasi at ETH Zurich, whose contributions are greatly acknowledged. The authors gratefully acknowledge the support by the staff of the structural engineering laboratory at ETH Zurich during the experiments; by the Chair of Durability of Engineering Materials at ETH Zurich, especially Dr. Carolina Boschmann Kaethler, for their help in microscopy; by the Chair of Geosensors and Engineering Geodesy at ETH Zurich, especially Robert Presl, for their help with the GOM Scanner; and by Laurent Mathez and Pirmin Schuler from Debrunner Acifer in organising the test samples. The study was partially funded by the Swiss Federal Roads Office and the Swiss Federal Office of Transport (Project AGB 2015/028).

References

[1] J. Cairns, G.A. Plizzari, Y. Du, D.W. Law, C. Franzoni, Mechanical Properties of corrosion-damaged reinforcement, ACI Mater. J. 102 (2005) 256–264.

[2] C. Apostolopoulos, G. Konstantopoulos, K. Koulouris, Seismic resistance prediction of corroded S400 (BSt420) reinforcing bars, IJSI 9 (1) (2018) 119–138, https://doi.org/10.1108/IJSI-02-2017-0008.

[3] C. Alk, K.F. Apostolopoulos, A.C. Koulouris, Apostolopoulos, Correlation of Surface Cracks of Concrete due to Corrosion and Bond Strength (between Steel Bar and Concrete), Adv. Civ. Eng. (2019 (2019)) 1–12, https://doi.org/10.1155/2019/3438743.

[4] Juraj Bilcik, Ivan Holly, Effect of Reinforcement Corrosion on Bond Behaviour, Procedia Eng. 65 (2013) 248–253, https://doi.org/10.1016/j.proeng.2013.09.038.
[5] fib fédération internationale du béton, Bond of reinforcement in concrete, fib Bulletin 10, 2000.
[6] Luisa Berto, Paola Simioni, Anna Saetta, Numerical modelling of bond behaviour in RC structures affected by reinforcement corrosion, Eng. Struct. 30 (5) (2008) 1375–1385, https://doi.org/10.1016/j.engstruct.2007.08.003.
[7] P. Lampert, A. Wegmüller, B. Thürlimann, Einfluss der Dehngeschwindigkeit auf Festigkeitswerte von Armierungsstählen, Schweiz. Bauztg. 85 (1967).
[8] E. Krempl, An experimental study of room-temperature rate-sensitivity, creep and relaxation of AISI type 304 stainless steel, J. Mech. Phys. Solids 27 (5-6) (1979) 363–375, https://doi.org/10.1016/0022-5096(79)90020-6.
[9] S. Haefliger, S. Fomasi, W. Kaufmann, Influence of quasi-static strain rate on the stress-strain characteristics of modern reinforcing bars, Construction and Building Materials. in press (2021).
[10] B. Hortigón Fuentes, J.M. Gallardo Fuentes, P. Gümpel, J. Strittmacher, Wirkung der Tempcore-Behandlung auf die Zugeigenschaften von Stabstahl, Stahl Eisen. 138 (2018).
[11] Ignasi Fernandez, Jesús Miguel Bairán, Antonio R. Marí, Mechanical model to evaluate steel reinforcement corrosion effects on σ – ε and fatigue curves. Experimental calibration and validation, Eng. Struct. 118 (2016) 320–333, https://doi.org/10.1016/j.engstruct.2016.03.055.
[12] José Santos, A. Abel Henriques, Strength and ductility of damaged tempcore rebars, Procedia Eng. 114 (2015) 800–807, https://doi.org/10.1016/j.proeng.2015.08.029.
[13] Ch. Alk. Apostolopoulos, G. Diamantogiannis, Alk. Ch. Apostolopoulos, Assessment of the mechanical behavior in dual-phase Steel B400C, B450C, and B500B in a marine environment, J. Mater. Civ. Eng. 28 (2) (2016) 04015097, https://doi.org/10.1061/(ASCE)MT.1943-5533.0001271.
[14] C. Apostolopoulos, A. Drakakaki, A. Apostolopoulos, T. Matikas, A.I. Rudskoi, G. Kodzhaspirov, Characteristic defects-corrosion damage and mechanical behavior of dual phase rebar, Mater. Phys. Mech. 30 (2017) 19.
[15] R. Hingorani, F. Pérez, J. Sánchez, J. Fullea, C. Andrade, P. Tanner, Loss of ductility and strength of reinforcing steel due to pitting corrosion, VIII International Conference on Fracture Mechanics of Concrete and Concrete Structures, Toledo, 2013. http://www.framcos.org/FraMCoS-8/p450.pdf (accessed September 1, 2015).
[16] Wenjun Zhu, Raoul François, Chi Sun Poon, Jian-Guo Dai, Influences of corrosion degree and corrosion morphology on the ductility of steel reinforcement, Constr. Build. Mater. 148 (2017) 297–306, https://doi.org/10.1016/j.conbuildmat.2017.05.079.
[17] C.A. Apostolopoulos, V.G. Papadakis, Consequences of steel corrosion on the ductility properties of reinforcement bar, Constr. Build. Mater. 22 (12) (2008) 2316–2324, https://doi.org/10.1016/j.conbuildmat.2007.10.006.
[18] Y.G. Du, L.A. Clark, A.H C. Chan, Effect of corrosion on ductility of reinforcing bars, Mag. Concr. Res. 57 (7) (2005) 407–419, https://doi.org/10.1680/macr.2005.57.7.407.
[19] Ignasi Fernandez, Jesús Miguel Bairán, Antonio R. Marí, Corrosion effects on the mechanical properties of reinforcing steel bars. Fatigue and σ–ε behavior, Constr. Build. Mater. 101 (2015) 772–783, https://doi.org/10.1016/j.conbuildmat.2015.10.139.
[20] S. Imperatore, Z. Rinaldi, Mechanical behaviour of corroded rebars and influence on the structural response of R/C elements, in: Concr. Repair Rehabil. Retrofit. II, CRC Press, Kapstadt, 2009.
[21] Alexander Baumgartner, Andreas Fraundorfer, Christoph Dauberschmidt, Andrea Kustermann, Veränderung der mechanischen Kenngrößen von Betonstabstählen durch chloridinduzierte Korrosion, Beton- und Stahlbetonbau 114 (6) (2019) 409–418, https://doi.org/10.1002/best.201900009.
[22] Mohammad M. Kashani, Adam J. Crewe, Nicholas A. Alexander, Use of a 3D optical measurement technique for stochastic corrosion pattern analysis of reinforcing bars subjected to accelerated corrosion, Corros. Sci. 73 (2013) 208–221, https://doi.org/10.1016/j.corsci.2013.03.037.
[23] I. Finozzi, A. Saetta, H. Budelmann, Structural response of reinforcing bars affected by pitting corrosion: experimental evaluation, Constr. Build. Mater. 192 (2018) 478–488, https://doi.org/10.1016/j.conbuildmat.2018.10.088.
[24] Dawang Li, Ren Wei, L. Li, Xiaotao Guan, Xuming Mi, Pitting corrosion of reinforcing steel bars in chloride contaminated concrete, Constr. Build. Mater. 199 (2019) 359–368, https://doi.org/10.1016/j.conbuildmat.2018.12.003.
[25] K. Andisheh, A. Scott, A. Palermo, Modeling the influence of pitting corrosion on the mechanical properties of steel reinforcement: Modeling the influence of pitting corrosion, Mater. Corros. 67 (11) (2016) 1220–1234, https://doi.org/10.1002/maco.201508795.
[26] A. Bautista, J.C. Pomares, M.N. González, F. Velasco, Influence of the microstructure of TMT reinforcing bars on their corrosion behavior in concrete with chlorides, Constr. Build. Mater. 229 (2019) 116899, https://doi.org/10.1016/j.conbuildmat.2019.116899.
[27] Charis Apostolopoulos, Structural integrity problems in dual-phase high ductility steel bar, J. Appl. Mech. Eng. 02 (01) (2013), https://doi.org/10.4172/2168-9873.1000115.
[28] D. Russwurm, Betonstähle für den Stahlbetonbau, Bauverlag, Wiesbaden und Berlin, 1993.
[29] Ezio Cadoni, Matteo Dotta, Daniele Forni, Nicoletta Tesio, Carlo Albertini, Mechanical behaviour of quenched and self-tempered reinforcing steel in tension under high strain rate, Mater. Des. 49 (2013) 657–666, https://doi.org/10.1016/j.matdes.2013.02.008.
[30] Marina Rocha, Eugen Brühwiler, Alain Nussbaumer, Geometrical and Material Characterization of Quenched and Self-Tempered Steel Reinforcement Bars, J. Mater. Civ. Eng. 28 (6) (2016) 04016012, https://doi.org/10.1061/(ASCE)MT.1943-5533.0001355.
[31] B.L. Bramfitt, O. Arlan, Metallographer's Guide – Practices and Procedures for Irons and Steels, 1st ed., ASM International, Materials Park OH, 2002.
[32] J. Rösler, H. Harders, M. Bäker, Mechanisches Verhalten der Werkstoffe, 3rd ed., Vieweg + Teubner, Wiesbaden, 2008.
[33] Karl-August Reckling (Ed.), Plastizitätstheorie und ihre Anwendung auf Festigkeitsprobleme, Springer Berlin Heidelberg, Berlin, Heidelberg, 1967.
[34] R.W.K. Honeycombe, The Plastic Deformation of Metals, Second Edition., Edward Arnold, London, 1984.